

Physics informed data-driven near-wall modelling for lattice Boltzmann simulation of high Reynolds number turbulent flows

Xiao Xue,^{1,2} Shuo Wang,³ Hua-Dong Yao,¹ Lars Davidson,¹ and Peter V. Coveney^{2, 4, 5, a)}

¹⁾*Division of Fluid Dynamics, Department of Mechanics and Maritime Sciences, Chalmers University of Technology, 41296, Gothenburg, Sweden*

²⁾*Centre for Computational Science, Department of Chemistry, University College London, London, UK*

³⁾*Fluids & Flows Group, Department of Applied Physics, Eindhoven University of Technology, The Netherlands*

⁴⁾*Informatics Institute, University of Amsterdam, The Netherlands*

⁵⁾*Centre for Advanced Research Computing, University College London, UK*

(Dated: 14 February 2024)

Data-driven approaches offer novel opportunities for improving the performance of turbulent flow simulations, which are critical to wide-ranging applications from wind farms and aerodynamic designs to weather and climate forecasting. While conventional continuum Navier-Stokes solvers have been the subject of a significant amount of work in this domain, there has hitherto been very limited effort in the same direction for the more scalable and highly performant lattice Boltzmann method (LBM), even though it has been successfully applied to a variety of turbulent flow simulations using large-eddy simulation (LES) techniques. In this work, we establish a data-driven framework for the LES-based lattice Boltzmann simulation of near-wall turbulent flow fields. We do this by training neural networks using improved delayed detached eddy simulation data. Crucially, this is done in combination with physics-based information that substantially constrains the data-driven predictions. Using data from turbulent channel flow at a friction Reynolds number at 5200, our simulations accurately predict the behaviour of the wall model at arbitrary friction Reynolds numbers up to 1.0×10^6 . In contradistinction with other models that use direct numerical simulation datasets, our physics-informed model requires data from very limited regions within the wall-bounded plane, reducing by three orders of magnitude the quantity of data needed for training. We also demonstrate that our model can handle data configurations when the near-wall grid is sparse. Our physics-informed neural network approach opens up the possibility of employing LBM in combination with highly specific and therefore much more limited quantities of macroscopic data, substantially facilitating the investigation of a wide-range of turbulent flow applications at very large scale.

Keywords: Physics-informed neural networks, wall model, lattice Boltzmann method, large-eddy-simulation

^{a)}Electronic mail: p.v.coveney@ucl.ac.uk

I. INTRODUCTION

Wall-modelled large-eddy simulations (WMLES) are crucial in within industrial design aerodynamics-driven applications such as aircraft, high-speed trains and wind turbines^{1,2}. These simulations provide a balance between computational efficiency and the resolution of flow physics. Although large-eddy simulations (LES) require fewer computational grid points than direct numerical simulations (DNS), wall-resolved LES necessitates fine grid resolution near the wall. The grid point requirement scales with $O(Re^{13/7})^{3-5}$. To expedite the aerodynamics-driven design process, WMLES emerges as a viable alternative to reduce computational costs significantly. Accurate modelling of the near-wall fluid field is imperative to maintain coarse-grained near-wall field resolution without compromising the accuracy of far-field physics. Traditionally, the near-wall field is modelled using the law of wall or by solving thin-boundary-layer equations⁶⁻⁹. In the current era of big data, the increasing availability of DNS data promotes machine learning and data-driven approaches to accurately capture the physics of coarse-grained models¹⁰.

Data-driven approaches based on machine learning (ML) have been widely used in industrial processes¹¹, computer vision¹² and control related problems^{13,14}. Recently, the data-driven approach has been employed for subgrid scale (SGS) modelling¹⁵⁻¹⁹ and near wall modelling^{20,21}. A common limitation of data-driven approaches is their lack of generality which stems from an inadequate understanding of the underlying physics. This limitation is evident when trained ML-based models show excellent ability to predict scenarios they have been trained on, sometimes referred to as “seen scenarios” or “interpolated schemes”, yet, struggle to predict “unseen scenarios” or “extrapolated schemes”, which fall outside the scope of their training data. A physics-informed data-driven approach offers a way of more effectively utilising datasets by embedding physical principles within the training process. Numerous studies have successfully implemented Physics-Informed Neural Networks (PINNs) for investigating turbulent flows using DNS data²¹⁻²⁴. While effective, these methods rely on DNS data which is not only computationally demanding to produce but also requires substantial storage capacity. In contrast, Bae and Koumoutsakos²⁰ employed multi-agent reinforcement learning to model the near-wall field in turbulent flows using hybrid Reynolds-Averaged Navier-Stokes (RANS)/LES data. The process of generating training data engenders a notable reduction in both computational and storage demands,

particularly when contrasted with techniques that depend on DNS data. Such methods are invariably based on the Computational Fluid Dynamics (CFD) approaches to solve the Navier-Stokes equations. The Lattice Boltzmann Method (LBM) by contrast, is recognized for its ability to model complex fluid phenomena across multiple scales, from microscopic²⁵⁻²⁹ to macroscopic³⁰⁻³³. Instead of solving the Navier-Stokes (NS) equations, LBM offers an alternative to conventional CFD methods by solving the Boltzmann equation at a mesoscopic level³³⁻³⁶. LBM is favoured for its parallelization-friendly characteristics, primarily due to the localized updating of discrete single particle distribution functions. Through the application of a Chapman-Enskog analysis to the Boltzmann equation, it is possible to derive the Navier-Stokes equations. Hou et al.³⁰ were instrumental in integrating the LES-based approach with LBM, particularly in modelling effective turbulent viscosity. As for near-wall modelling in LBM, Malaspinas et al.³⁷ demonstrated the successful reconstruction of first-layer near-wall velocity with a regularized scheme³⁸ using the Musker wall function or logarithmic law³⁹. Subsequent research focused on reconstructing the velocity field or modelling velocity bounce-back^{37,40-42}. The forcing-based method, noted for its simplicity, has also been applied in modelling the near-wall fluid field^{43,44}.

To date, existing data-driven wall models have been developed within the Navier-Stokes (NS) framework. However, there is no established data-driven approach that models the near-wall fluid field using the LBM framework. This paper presents a methodology for utilizing both grid-intensive and grid-sparse improved delayed detached eddy simulation (IDDES)⁴⁵ data to develop a generalized neural network(NN) wall model within the lattice Boltzmann framework. In the current study, IDDES data is trained at friction Reynolds number, Re_τ , equal to $Re_\tau = 5200$. Subsequently, this data is applied to the NN wall model for turbulent channel flow, incorporating a synthetic turbulent generator (STG) at the inlet as described by Xue et al.⁴⁶, at $Re_\tau = 1000, 2000, 5200$. The results show good agreement with DNS data at coarse resolutions with the channel height of 20 lattice grid separations. To highlight the model's generality, we further validate our NN wallmodel for the LBM based turbulent channel flow at the friction Reynolds number $Re_\tau = 1.0 \times 10^5$ and $Re_\tau = 1.0 \times 10^6$. It is noteworthy that the grid-intensive data used in this study amounts to only 45 megabytes (MBs) while the grid-sparse data is even more compact, requiring just 6.4 MBs, in contrast to DNS data, which can range from hundreds of gigabytes (GBs) to several terabytes (TBs). Our work illustrates the benefits of integrating data-driven approaches with physical knowl-

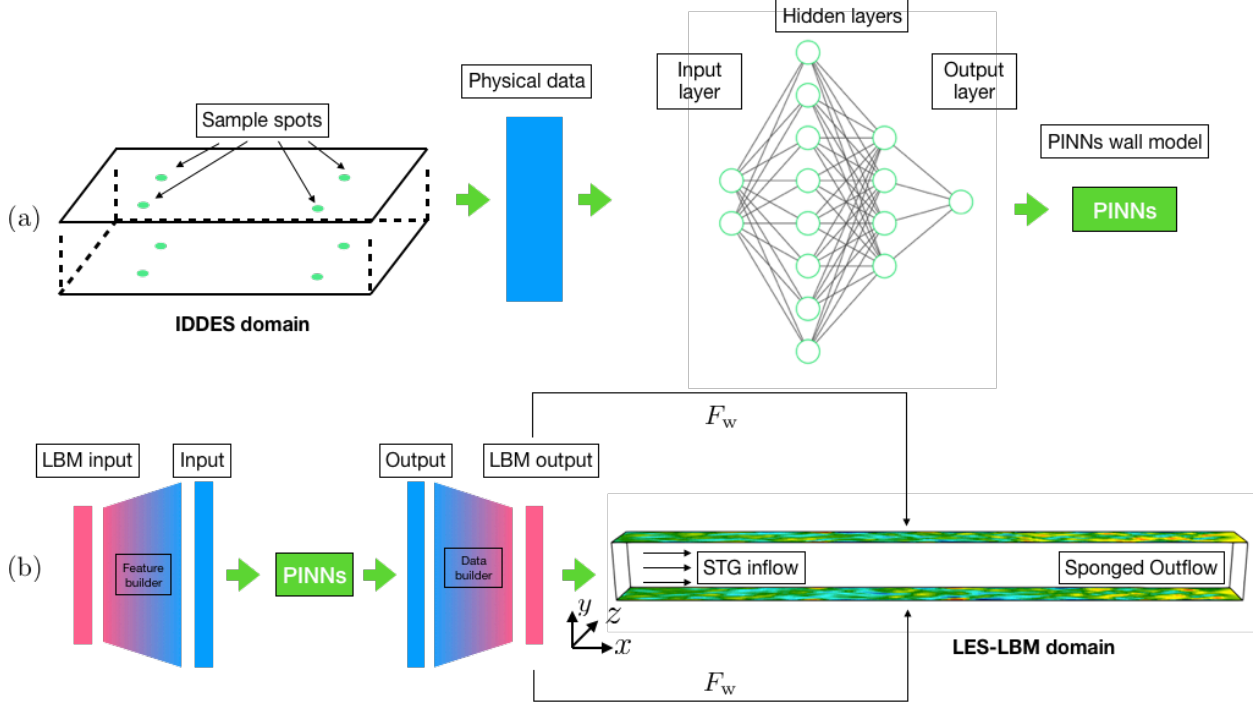


FIG. 1. Diagram of the physics-informed neural network architecture and implementation for the lattice Boltzmann method trained by IDDES data at $Re_\tau = 5200$. Panel (a): the training data is obtained from the upper and lower near-wall region of a periodic channel flow simulation. We use NN to predict the shear velocity which can be used by the wall model. Panel (b): LES based LBM channel flow simulation is performed, on the first layer of the wall, we use the LBM data as the input. With the help of the pre-trained PINNs wall model, we can predict LBM shear velocity to calculate the resistance wall force F_w for the wall model.

edge to model the near-wall dynamics in the lattice Boltzmann method. We demonstrate here that this approach can leverage CFD data very effectively in the context of NN-based wall modelling within the lattice Boltzmann framework.

II. RESULTS

A. Physics-informed neural network wall modelling framework for LBM

As shown in Fig. 1 (a), we uniformly sample the upper and lower panels of the IDDES periodic channel flow⁴⁵ at grid points where $y^+ < 200$. Here, y^+ represents the dimensionless wall-normal distance, defined as $y^+ = \frac{yu_\tau}{\nu}$, where ν denotes the kinematic viscosity and

u_τ is the shear velocity. We ensure consistency in the sampling locations across different instantaneous snapshots for the channel flow simulations. The IDDES simulation of turbulent channel flow is conducted at $Re_\tau = 5200$. Owing to the varying grid density near the wall, the sampled data may range from dense to sparse. Our primary objective is the accurate prediction of the shear velocity, u_τ , to reliably estimate wall velocities. It is crucial to recognize that the grids used in IDDES are distinct from those in lattice Boltzmann configurations. In contrast to conventional CFD methodologies, the LBM utilizes a uniform grid structure and is formulated with dimensionless variables. This distinction in grid structure necessitates precise capture of the physics inherent in the near-wall region. Figure 1 (b) illustrates the pipeline for applying a neural network wall model to LBM turbulent channel flow. The coordinates of the LBM channel flow are denoted as x, y, z , corresponding to the stream-wise, vertical, and span-wise directions, respectively. Turbulent flow is initiated with the synthetic turbulence generation (STG) method at the inlet, while the outlet features a sponge region⁴⁶. The domain dimensions of the turbulent channel flow are $L_x \times L_y \times L_z$, measuring $320 \times 20 \times 16$ lattice Boltzmann units (LBU). The upper and lower boundaries of the channel employ a free-slip condition. The near-wall region is modelled using a volume force predicted by neural networks. The process involves converting LBM data into PINNs feature input with the help of a feature builder, followed by predicting the feature output of shear velocity. Subsequently, this prediction is converted back into LBM data with the help of a data builder to compute the resistive volume force, thereby correcting near-wall velocities. In the feature builder, a normalizer and LBM-to-physical unit converter are utilized to ensure that input values consistently fall within the range $[0, 1]$. The data builder consists of a de-normalizer and a physical-to-LBM unit converter. A detailed description of the NN model is provided in Section IV E and Section IV F.

B. Dense-data wall model vs sparse-data wall model

Due to varying grid density near the wall in IDDES data, “gaps” may exist between data points. As shown in Fig. 2 (a), blue dots represent dense data, indicating densely arranged grids below $y^+ < 200$ near the wall. The application of neural networks (NN) to learn wall functions from data is demonstrated. The orange line confirms that NNs accurately capture the wall functions at $y^+ < 200$. This NN model, which requires no data correction,

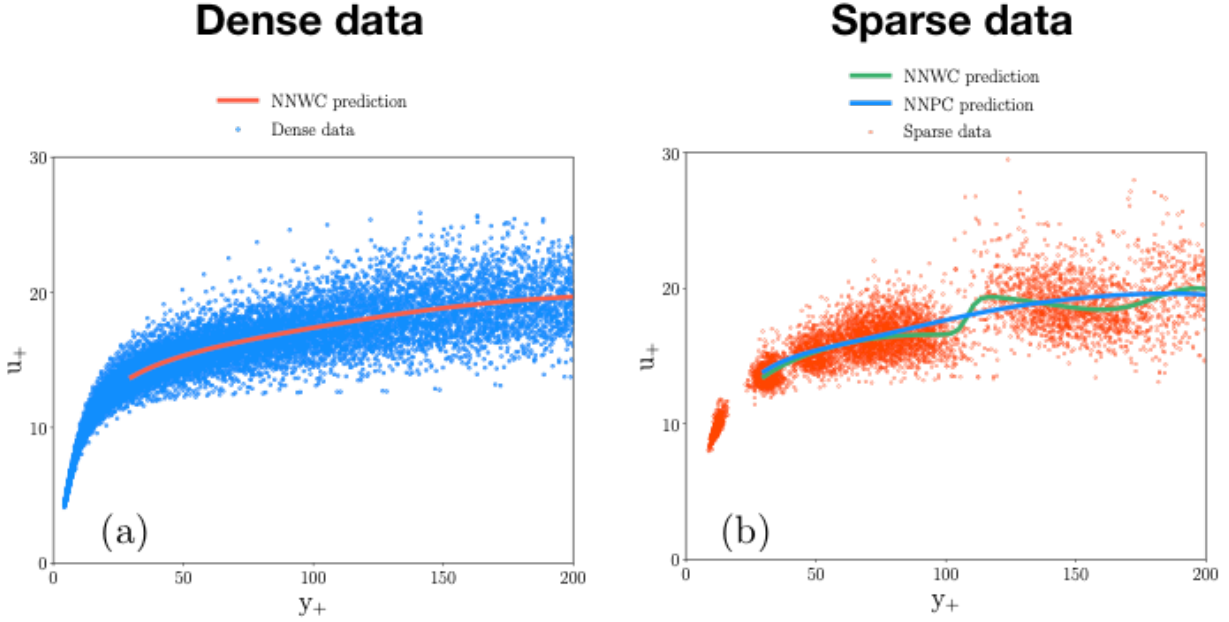


FIG. 2. Diagram of NN learning the law of wall at $y^+ < 200$ with IDDES data. Panel (a): demonstrates dense data configuration (blue dots) with u^+ as function of y^+ . NNWC prediction is illustrated by the orange line. Panel (b): demonstrates sparse data configuration (orange dots) comparing NNWC and NNPC predictions.

is thus referred to as the “NNWC” model (Neural Networks Without PDF Correction). The NNWC model’s predictions correspond closely with the IDDES data. In Fig. 2 (b), orange dots represent sparsely configured grids near the wall, enhancing computational efficiency. However, the direct application of the NNWC model to sparse data, as depicted by the dark green line, risks overfitting and creating a staggered wall function. To mitigate this, we apply PDF corrections, minimizing the impact of “gap” regions between data groups during training (see Section IV F). As shown by the blue line, the NNPC model (Neural Networks with PDF Correction) can precisely capture the law of the wall even with sparse training data.

Figure 3 (a) depicts the Absolute Relative Error (ARE) in predicting shear velocity, u_τ , using neural networks on IDDES data, comparing both the NNWC and NNPC models. The blue curve illustrates the ARE of the NNWC model’s predictions for dense data. This error notably decreases to 2% around $y^+ \approx 200$, reflecting the model’s training on datasets below

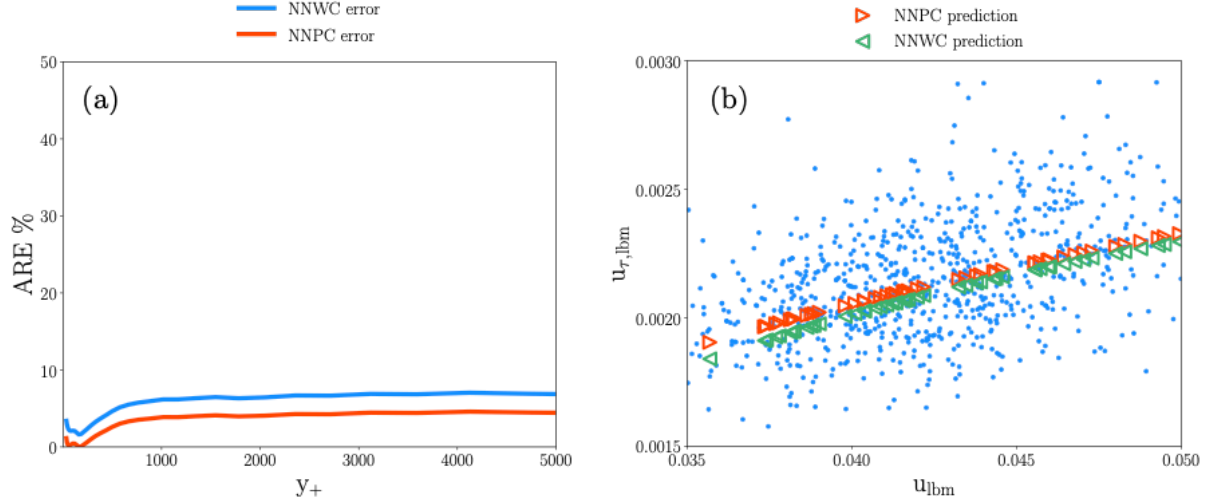


FIG. 3. Panel (a): absolute relative error (ARE) for u_{τ} prediction based on IDDES simulations for y^+ up to 5200 with or without PDF correction. Panel (b): LBM data prediction on shear velocity $u_{\tau,lbm}$ with input of LBM velocity u_{lbm} at $y^+ = 260$ for the channel flow simulation at $Re_{\tau} = 5200$. Blue dots represents the LBM data, the NNPC and NNWC model predictions are represented by the red and green triangular dots respectively.

$y^+ = 200$. Beyond this point, the ARE rises to 6% but remains stable up to $y^+ = 5000$. Conversely, the orange curve represents the ARE of the NNPC model for sparse data. With the application of PDF correction, the ARE drops below 1% near $y^+ \approx 200$. Despite a slight increase in ARE beyond $y^+ = 200$, it stabilizes at around 4% for $y^+ \leq 5000$. The NNPC model demonstrates an accuracy improvement of 2% over the NNWC model. In Fig. 3 (b), orange triangles represent NNPC predictions, while green triangles are indicative of NNWC predictions. Both models exhibit good alignment with the LBM data. Based on the findings in Fig. 2 and Fig. 3, the NNWC model is selected for interpolation and extrapolation tests in LBM channel flow simulations.

C. Interpolation validation for the neural network wall model up to $Re_{\tau} = 5200$

The turbulent channel flow serves as the validation case for the neural network wall model. In this setup, the channel flow employs a LBM-based synthetic turbulence generator at the inlet, as described in⁴⁶, and incorporates a sponge layer at the outlet. The volume force, $F_w(\mathbf{x}, t)$, exerted on the first layer of cells near the wall, can be characterized at location \mathbf{x}

as

$$F_w(\mathbf{x}, t) = -\tau_w(\mathbf{x}, t)A, \quad (1)$$

where τ_w can be obtained by shear velocity and density: $\tau_w(\mathbf{x}, t) = u_{\tau, \text{lbm}}^2(\mathbf{x}, t)\rho(\mathbf{x}, t)$. A is the acting area. The height of the channel is set to 20 LBU. Consequently, the y^+ values of the first cell layer for friction Reynolds numbers $Re_\tau = 1000, 2000, \text{ and } 5200$ are approximately 50, 100, and 260, respectively. These results are benchmarked against DNS data from^{47,48}. Owing to the rapid convergence characteristics of the turbulence generator⁴⁶, simulations are executed at various friction Reynolds numbers. Each simulation runs for a total duration of 12 domain-through-times ($12T$), with statistical analyses commencing post $2T$. The cross-section sampling is performed at $x/\delta = 8$ to ensure robust statistical properties of the turbulence, where δ is the turbulent boundary layer thickness and is equal to $\delta = 10$ LBU for the channel flow case. Figure 4 (a) illustrates the mean flow velocity u^+ of LBM turbulent flow as a function of y^+ . The red, blue, and green dots correspond to LBM simulations at $Re_\tau = 1000, 2000, 5200$, respectively. The black dotted line represents the DNS data at $Re_\tau = 5200$. The results of our LBM NNPC-based wall model demonstrate good alignment with the DNS data. Subsequently, the turbulent shear stress $\langle u'v' \rangle^+$ is compared with the DNS reference data. Figure 4 (b) displays $\langle u'v' \rangle^+$ as a function of y/δ for $Re_\tau = 1000, 2000, 5200$. The red, blue, and green dotted lines represent the DNS references^{47,48}, while the corresponding coloured points denote the LBM NNPC-based wall model results. Discrepancies are observed in the first three cells near the wall, attributable to coarse-grained resolution issues, given that the channel height comprises only 20 lattice units. Beyond the fourth grid cell, the LBM results closely match the DNS data, indicating the efficacy of our wall model in accurately capturing the physics of the turbulent stress tensor in channel flow.

D. Extrapolation studies for the neural network wall model up to

$$Re_\tau = 1.0 \times 10^6$$

To demonstrate the generality of our NNPC-based wall model, we extended its application to friction Reynolds numbers $Re_\tau = 1.0 \times 10^5$ and $Re_\tau = 1.0 \times 10^6$, which are two orders of magnitude higher than those considered in previous LBM-base wall model studies^{37,40–42,49}.

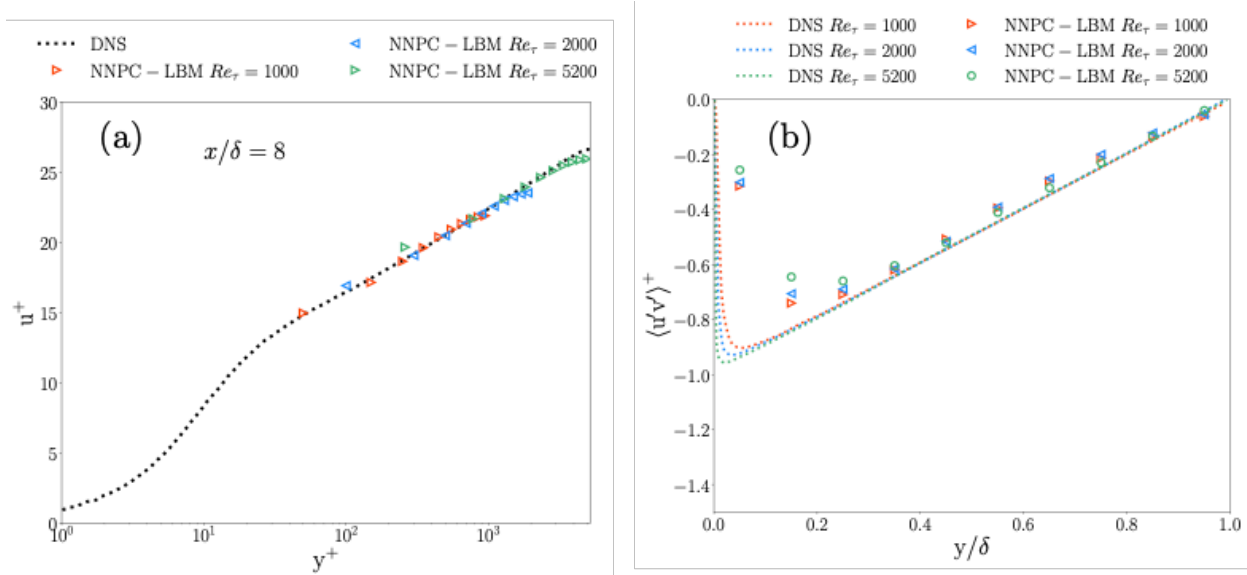


FIG. 4. Interpolation validation for turbulent channel flow up to $Re_\tau = 5200$. Panel (a): Mean velocity, u^+ , as function of y^+ at $Re_\tau = 1000, 2000, 5200$. Panel (b): $\langle u'v' \rangle^+$ as function of y/δ at $Re_\tau = 1000, 2000, 5200$

For channel flow simulations at these elevated Reynolds numbers, the first cell layer of the NNPC-based model corresponds to approximately $y^+ = 5000$ and $y^+ = 50000$, respectively, significantly exceeding the range of the initial training dataset.

Figure 5 presents u^+ as a function of y^+ for $Re_\tau = 1.0 \times 10^5$ and 1.0×10^6 . The black dotted line represents the DNS reference at $Re_\tau = 5200$. Due to the absence of DNS data for these higher Reynolds numbers, the green dotted line depicts the universal logarithmic wall law (Log WL), which is expressed as

$$u^+ = 1/\kappa \log y^+ + B, \quad (2)$$

where κ is chosen to be 0.42 and B is set to 5.2. The purple and yellow dots represent the LBM-based NNPC wall model results at $Re_\tau = 1.0 \times 10^5$ and $Re_\tau = 1.0 \times 10^6$, respectively. Results from the channel flow simulations under $Re_\tau = 5200$ are also included in the figure, depicted in faded colours for comparative purposes. Although our neural network model is primarily guided by physical data, it aligns remarkably well with the logarithmic wall law up to $Re_\tau = 1.0 \times 10^6$. This concordance highlights the versatility and effectiveness of our NNPC-based wall model within the LBM framework.

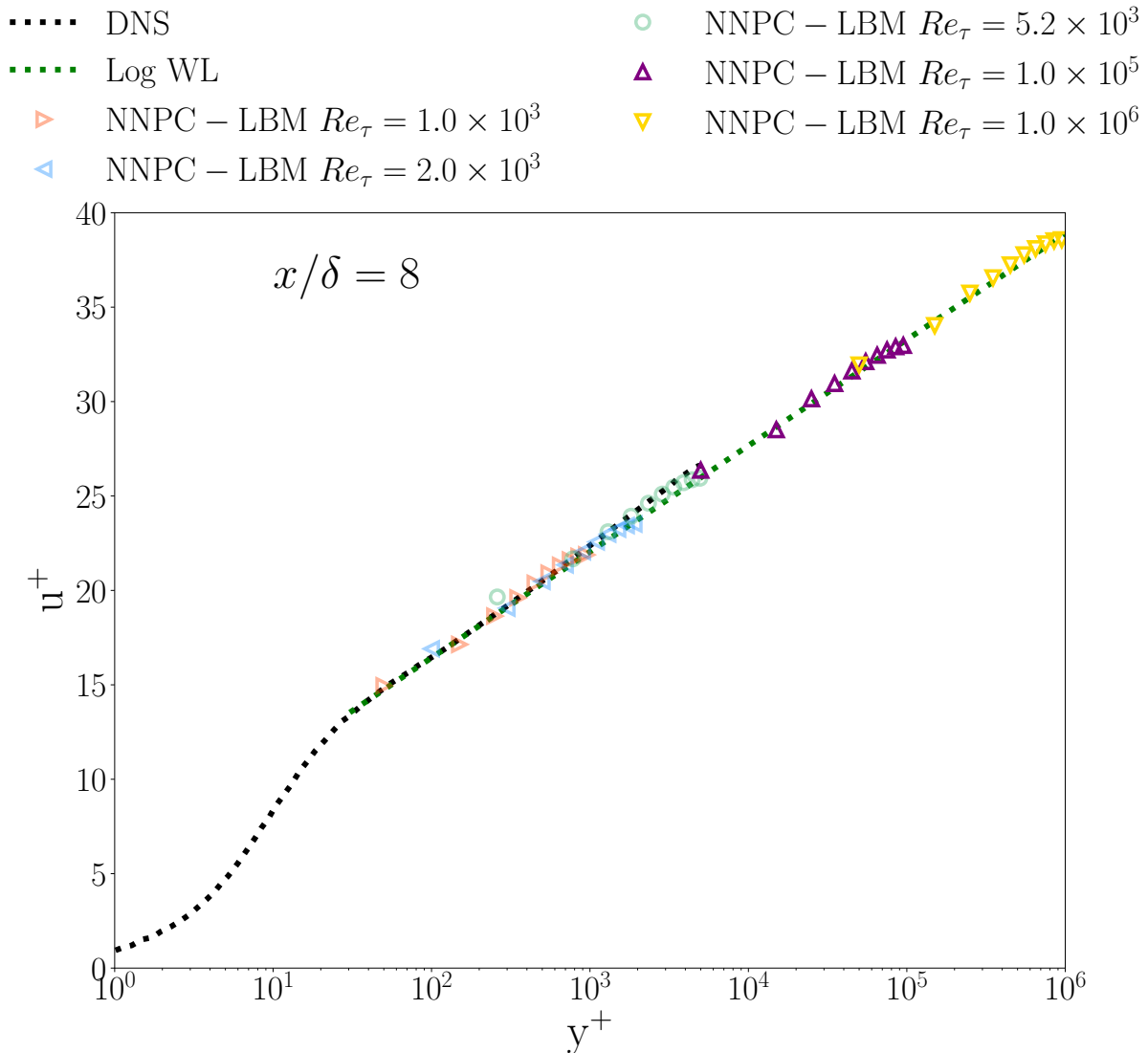


FIG. 5. Extrapolation validation: mean velocity u^+ as function of y^+ at $Re_\tau = 10^5$ (purple dots) and $Re_\tau = 10^6$ (yellow dots). The green dotted line is the log wall law satisfying Eq. (2), for which DNS data is only available up to $Re_\tau = 5200$.

III. CONCLUDING REMARKS

This paper introduces a physics-informed neural network wall model tailored for the lattice Boltzmann method. The model was trained using IDDES channel flow simulations at $Re_\tau = 5200$. Due to grid sparsity near the wall, the training dataset encompasses both dense and sparse data configurations below $y^+ = 200$. Implementing PDF corrections leads to a 2% reduction in error compared to models without such corrections, yielding an

approximate absolute relative error of 4% for $y^+ > 1000$. We evaluated our NNPC-based wall model in LBM channel flow simulations using STG as the inlet. Despite the coarse-grained nature of LBM channel flow, our simulation results align well with DNS data up to $Re_\tau = 5200$. It is noteworthy that previous LBM channel flow studies can only validate the wall model till $Re_\tau = 2.0 \times 10^{437}$. We further validate our NNPC-based LBM wall model with the logarithmic wall law at scale of $Re_\tau = 10^6$ where DNS data is not available. This evidence supports the conclusion that our NNPC-based wall model is effective for arbitrarily high friction Reynolds numbers. It should be noted that investigations beyond this range were not conducted as they exceed typical application requirements. Nonetheless, we are confident that the model will adhere to the logarithmic wall law even at higher friction Reynolds numbers. As a concluding remark, our novel NNPC-based wall-model demonstrates effective performance on coarse-grained grids near the wall. It is versatile enough to be applied to flows at arbitrarily high Reynolds numbers, opening up a broad array of aerodynamics-related industrial applications.

IV. METHODS

A. The multiple-relaxation time lattice Boltzmann method

This study employs a three-dimensional (3D) Lattice Boltzmann model featuring 19 discretized directions, known as the D3Q19 model. The lattice cell is specified by its position \mathbf{x} and time t , and is characterized by a discretized velocity set \mathbf{c}_i where $i \in \{0, 1, \dots, Q-1\}$ with $Q = 19$. Macro-scale quantities such as density, momentum, and momentum flux tensors are derived from the distribution function $f_i(\mathbf{x}, t)$, the discrete velocities \mathbf{c}_i , and the volume acceleration, \mathbf{g} :

$$\rho(\mathbf{x}, t) = \sum_{i=0}^{Q-1} f_i(\mathbf{x}, t), \quad (3)$$

$$\rho(\mathbf{x}, t)\mathbf{u}(\mathbf{x}, t) = \sum_{i=0}^{Q-1} f_i(\mathbf{x}, t)\mathbf{c}_i + \frac{1}{2}\mathbf{g}\Delta t, \quad (4)$$

$$\mathbf{\Pi}(\mathbf{x}, t) = \sum_{i=0}^{Q-1} f_i(\mathbf{x}, t)\mathbf{c}_i\mathbf{c}_i. \quad (5)$$

The evolution equation for the distribution functions, accounting for collision and forcing, can be expressed as:

$$\mathbf{f}(\mathbf{x} + \mathbf{c}_i \Delta t, t + \Delta t) = \mathbf{f}(\mathbf{x}, t) - \mathbf{\Omega} [\mathbf{f}(\mathbf{x}, t) - \mathbf{f}^{\text{eq}}(\mathbf{x}, t)] + \mathbf{F}(\mathbf{x}, t) \Delta t, \quad (6)$$

where $\mathbf{\Omega}$ denotes the multiple relaxation time (MRT) collision kernel, defined as $\mathbf{\Omega} = \mathbf{M}^{-1} \mathbf{S} \mathbf{M}^{50}$. The matrix \mathbf{S} is a diagonal matrix comprising relaxation frequencies for different moments, expressed as $\mathbf{S} = \text{diag}\{\omega_0, \omega_1, \dots, \omega_{Q-1}\}$. The matrix \mathbf{M} represents the transformation matrix that converts population space to moment space, derived using the Gram-Schmidt orthogonalization process. In Eq. (6), Δt symbolizes the lattice Boltzmann time step, which is standardized to unity. The frequency ω_i corresponds to the inverse of relaxation time τ_i . It is important to note that we equate $\tau_k = \tau_9 = \tau_{11} = \tau_{13} = \tau_{14} = \tau_{15}$, all of which are associated with the kinematic viscosity ν , which is

$$\nu = c_s^2 \left(\tau_k - \frac{1}{2} \right) \Delta t, \quad (7)$$

with c_s representing the speed of sound, and c_s^2 equating to $\frac{1}{3}$ in Lattice Boltzmann Units (LBU). The other relaxation parameters, which are not governed by the viscosity, are set as follows:

$$\omega_0 = \omega_3 = \omega_5 = \omega_7 = \omega_1 = 1.0 \quad (8)$$

$$\omega_1 = 1.19, \quad (9)$$

$$\omega_2 = \omega_{10} = \omega_{12} = 1.6 \quad (10)$$

$$\omega_4 = \omega_6 = \omega_8 = 1.2 \quad (11)$$

$$\omega_{16} = \omega_{17} = \omega_{18} = 1.98. \quad (12)$$

$\mathbf{F}(\mathbf{x}, t)$ in Eq. (6) is the vector of $F_i(\mathbf{x}, t)$ which is the force acting on the fluid cell⁵¹:

$$F_i(\mathbf{x}, t) = \left(1 - \frac{\omega_i}{2}\right) w_i \left[\frac{\mathbf{c}_i - \mathbf{u}(\mathbf{x}, t)}{c_s^2} + \frac{\mathbf{c}_i \cdot \mathbf{u}(\mathbf{x}, t)}{c_s^4} \mathbf{c}_i \right] \cdot \mathbf{g}. \quad (13)$$

B. Smagorinsky subgrid-scale modelling

In this part, we summarize the lattice-Boltzmann-based Smagorinsky Subgrid Scale (SGS) LES techniques. Within the LBM framework, the effective viscosity $\nu_{\text{eff}}^{30,52,53}$ is modelled as the sum of the molecular viscosity, ν_0 , and the turbulent viscosity, ν_t :

$$\nu_{\text{eff}} = \nu_0 + \nu_t, \quad \nu_t = C_{\text{smag}} \Delta^2 |\bar{\mathbf{S}}|, \quad (14)$$

where $|\bar{\mathbf{S}}|$ is the filtered strain rate tensor, C_{smag} is the Smagorinsky constant, Δ represents the filter size.

C. Synthetic turbulence generator formulation

The synthetic turbulence generator (STG) requires a velocity field given by a $k - \varepsilon$ Reynolds-Averaged Navier-Stokes (RANS) simulation⁵⁴. The total velocity $\mathbf{u}_{\text{in}}(\mathbf{x}, t)$ at the inlet is given by

$$\mathbf{u}_{\text{in}}(\mathbf{x}, t) = \mathbf{u}_{\text{RANS}}(\mathbf{x}) + \mathbf{u}'(\mathbf{x}, t), \quad (15)$$

where \mathbf{u}_{RANS} is the velocity vector obtained from a RANS simulation, then the interpolated velocity will be applied on LBM grid in case of grid resolution differences⁴⁶. The STG generates the velocity fluctuations $\mathbf{u}'(\mathbf{x}, t)$ at the cell \mathbf{x} at time t :

$$\mathbf{u}'(\mathbf{x}, t) = a_{\alpha\beta} \mathbf{v}'(\mathbf{x}, t). \quad (16)$$

The time-averaged velocity fluctuation is zero, i.e., $\langle \mathbf{u}'(\mathbf{x}, t) \rangle = 0$. The term $a_{\alpha\beta}$ represents the Cholesky decomposition of the Reynolds stress tensor. The fluctuations $\mathbf{v}'(\mathbf{x}, t)$ are imposed by N Fourier modes. Detailed descriptions of this process are available in Xue and co-authors⁴⁶.

D. IDDES database preparation

The finite volume code pyCALC-LES⁵⁵ is utilised, which is implemented in Python and fully vectorised. Spatial discretisation for the momentum equations employs a second-order central difference scheme, while temporal discretisation utilizes the Crank-Nicolson scheme. The evolution of the $k - \varepsilon$ RANS turbulence model adopts a hybrid central/upwind scheme, complemented by a first-order fully implicit time discretisation approach. The discretised equations, forming a sparse-matrix system, are solved on the GPU using the Algebraic Multi-Grid library pyAMGx⁵⁶. For turbulent data generation, the dimensions of the channel flow in the streamwise, wall-normal, and spanwise directions are set to $3.2 \times 2 \times 1.6$ meters,

NN model	HL size	Input	Output
NNPC & NNWC	(9, 9)	y^+	u^+
NNPC	(9, 8, 5)	$(\frac{u}{1000y}, \frac{y/y_{ref}}{u})$	u_τ

TABLE I. Details of the neural networks for law of wall prediction and shear velocity u_τ prediction. Here NN denotes neural network and HL denotes hidden layer. The tabulated hidden layer size contains the number of neurons within each hidden layer.

respectively. The computational mesh comprises $96 \times 96 \times 96$ cells, and the Reynolds number based on the friction velocity, Re_τ , is set to 5200.

E. Physics-informed neural networks for wall model

We use a PINN model that contains several fully connected hidden layers with the *tanh* function as activation function. Generally, the input is reformulated so that it provides crucial physics and helps to find a convergence in the optimization process when training the model.

The detailed description of our NN models are listed in Tab.I. The NNPC and NNWC models were both tested on predicting y^+ and u^+ . However, to ensure we identify a model with the generality to predict shear velocity u_τ , we need actual physics-informed input. We choose $u/(1000y)$ and $y/y_{ref}/u$ to learn the log scale slope of the log wall law in Eq. (2). The model outputs a continuous value in the interval $[0,1]$, which is linearly mapped to $[u_{\tau,min}, u_{\tau,max}]$ for further application.

F. Neural network training

We trained the PINNs model in a supervised fashion, with a loss function \mathcal{L} , consisting of L_2 norm and a weight function. The model is trained by a sample of size N , with a predicted vector \mathbf{X}_{PINNs} and target vector \mathbf{Y} , the total loss yields:

$$\mathcal{L} = \frac{1}{N} \sum_{n=1}^N w_{loss} \|\mathbf{Y} - \mathbf{X}_{PINNs}\|^2. \quad (17)$$

Here the weight function $w_{\text{loss}} = 1/[P_r(\mathbf{X}_{\text{PINNs}}) + \epsilon]$ compensates for the gaps in data points (as shown in Fig. Fig. 2 (a)). The constant $\epsilon = 10^{-6}$ avoids infinite value of the weight function. To provide a general solution to deal with the arbitrary “gap” on data sample, the weight function is also learned during the training process. An M -dimensional input data with N sample points is firstly normalized and linearly projected into interval $[0,1]$. Here, the M is number of inputs which is set to 2. The data range across each dimension is discretized into J uniform segments. Therefore, the likelihood of a data point being located in the j th segment of the i th dimension is quantified as

$$P(i, j_i) = \frac{N_{i,j}}{N}, \quad (18)$$

where $N_{i,j}$ denotes the number of training data falls in the j th segment in i th dimension. We use the expression

$$P_r(j_1, j_2 \dots j_M) = \prod_{i=1}^M P(i, j_i) \quad (19)$$

to denote the relative possibility of a data point that falls in the $(j_1, j_2 \dots j_M)$ segment. We pragmatically used $J = 100$ in the training phase.

The sparse dataset is uniformly sampled from a total of 10,000 input-output pairs. This dataset comprises 2,000 points that are uncorrelated in both time and space, gathered from five layers of grids from the IDDES channel flow simulations located under $y^+ < 200$. For the model trained on dense data, the dataset consists of 19,600 input-output pairs, sourced from the grids under $y^+ < 200$. We adopted a training-to-test ratio of 80% to 20%.

REFERENCES

- ¹F. Porté-Agel, Y.-T. Wu, H. Lu, and R. J. Conzemius, “Large-eddy simulation of atmospheric boundary layer flow through wind turbines and wind farms,” *Journal of Wind Engineering and Industrial Aerodynamics* **99**, 154–168 (2011).
- ²D. Mehta, A. Van Zuijlen, B. Koren, J. Holierhoek, and H. Bijl, “Large Eddy Simulation of wind farm aerodynamics: A review,” *Journal of Wind Engineering and Industrial Aerodynamics* **133**, 1–17 (2014).
- ³D. R. Chapman, “Computational aerodynamics development and outlook,” *AIAA journal* **17**, 1293–1313 (1979).

- ⁴H. Choi and P. Moin, “Grid-point requirements for large eddy simulation: Chapman’s estimates revisited,” *Physics of Fluids* **24**, 011702 (2012).
- ⁵X. I. Yang and K. P. Griffin, “Grid-point and time-step requirements for direct numerical simulation and large-eddy simulation,” *Physics of Fluids* **33**, 015108 (2021).
- ⁶U. Schumann, “Subgrid scale model for finite difference simulations of turbulent flows in plane channels and annuli,” *Journal of computational physics* **18**, 376–404 (1975).
- ⁷G. I. Park and P. Moin, “An improved dynamic non-equilibrium wall-model for large eddy simulation,” *Physics of Fluids* **26** (2014).
- ⁸J. Larsson, S. Kawai, J. Bodart, and I. Bermejo-Moreno, “Large eddy simulation with modeled wall-stress: recent progress and future directions,” *Mechanical Engineering Reviews* **3**, 15–00418 (2016).
- ⁹S. T. Bose and G. I. Park, “Wall-modeled large-eddy simulation for complex turbulent flows,” *Annual Review of Fluid Mechanics* **50**, 535–561 (2018).
- ¹⁰S. L. Brunton, B. R. Noack, and P. Koumoutsakos, “Machine learning for fluid mechanics,” *Annual Review of Fluid Mechanics* **52**, 477–508 (2020).
- ¹¹S. Yin, S. X. Ding, X. Xie, and H. Luo, “A review on basic data-driven approaches for industrial process monitoring,” *IEEE Transactions on Industrial electronics* **61**, 6418–6428 (2014).
- ¹²K. Gopalakrishnan, S. K. Khaitan, A. Choudhary, and A. Agrawal, “Deep convolutional neural networks with transfer learning for computer vision-based data-driven pavement distress detection,” *Construction and building materials* **157**, 322–330 (2017).
- ¹³S. X. Ding, *Data-driven design of fault diagnosis and fault-tolerant control systems* (Springer London, 2014).
- ¹⁴Z.-S. Hou and Z. Wang, “From model-based control to data-driven control: Survey, classification and perspective,” *Information Sciences* **235**, 3–35 (2013).
- ¹⁵F. Sarghini, G. De Felice, and S. Santini, “Neural networks based subgrid scale modeling in large eddy simulations,” *Computers & fluids* **32**, 97–108 (2003).
- ¹⁶M. Gamahara and Y. Hattori, “Searching for turbulence models by artificial neural network,” *Physical Review Fluids* **2**, 054604 (2017).
- ¹⁷J.-L. Wu, H. Xiao, and E. Paterson, “Physics-informed machine learning approach for augmenting turbulence models: A comprehensive framework,” *Physical Review Fluids* **3**, 074602 (2018).

- ¹⁸C. Xie, J. Wang, H. Li, M. Wan, and S. Chen, “Artificial neural network mixed model for large eddy simulation of compressible isotropic turbulence,” *Physics of Fluids* **31** (2019).
- ¹⁹S. Cai, Z. Wang, F. Fuest, Y. J. Jeon, C. Gray, and G. E. Karniadakis, “Flow over an espresso cup: inferring 3-d velocity and pressure fields from tomographic background oriented Schlieren via physics-informed neural networks,” *Journal of Fluid Mechanics* **915**, A102 (2021).
- ²⁰H. J. Bae and P. Koumoutsakos, “Scientific multi-agent reinforcement learning for wall-models of turbulent flows,” *Nature Communications* **13**, 1443 (2022).
- ²¹X. Yang, S. Zafar, J.-X. Wang, and H. Xiao, “Predictive large-eddy-simulation wall modeling via physics-informed neural networks,” *Physical Review Fluids* **4**, 034602 (2019).
- ²²M. Raissi, P. Perdikaris, and G. E. Karniadakis, “Physics-informed neural networks: A deep learning framework for solving forward and inverse problems involving nonlinear partial differential equations,” *Journal of Computational physics* **378**, 686–707 (2019).
- ²³J.-X. Wang, J.-L. Wu, and H. Xiao, “Physics-informed machine learning approach for reconstructing Reynolds stress modeling discrepancies based on dns data,” *Physical Review Fluids* **2**, 034603 (2017).
- ²⁴L. Davidson, “Using machine learning for formulating new wall functions for Large Eddy Simulation: A second attempt,” Div. of Fluid Dynamics, Mechanics and Maritime Sciences, Chalmers University of Technology (2022).
- ²⁵X. Xue, L. Biferale, M. Sbragaglia, and F. Toschi, “A lattice Boltzmann study on Brownian diffusion and friction of a particle in a confined multicomponent fluid,” *Journal of Computational Science* **47**, 101113 (2020).
- ²⁶X. Xue, M. Sbragaglia, L. Biferale, and F. Toschi, “Effects of thermal fluctuations in the fragmentation of a nanoligament,” *Physical Review E* **98**, 012802 (2018).
- ²⁷X. Xue, L. Biferale, M. Sbragaglia, and F. Toschi, “A lattice Boltzmann study of particle settling in a fluctuating multicomponent fluid under confinement,” *The European Physical Journal E* **44**, 1–10 (2021).
- ²⁸D. Chiappini, X. Xue, G. Falcucci, and M. Sbragaglia, “Ligament break-up simulation through pseudo-potential lattice Boltzmann method,” in *AIP Conference Proceedings*, Vol. 1978 (AIP Publishing, 2018) p. 420003.
- ²⁹D. Chiappini, M. Sbragaglia, X. Xue, and G. Falcucci, “Hydrodynamic behavior of the pseudopotential lattice Boltzmann method for interfacial flows,” *Physical Review E* **99**,

- 053305 (2019).
- ³⁰S. Hou, J. Sterling, S. Chen, and G. Doolen, “A lattice Boltzmann subgrid model for high Reynolds number flows,” *Pattern formation and lattice gas automata*, 151–166 (1995).
- ³¹F. Toschi and E. Bodenschatz, “Lagrangian properties of particles in turbulence,” *Annual Review of Fluid Mechanics* **41**, 375–404 (2009).
- ³²I. V. Karlin, A. Ferrante, and H. C. Öttinger, “Perfect entropy functions of the lattice Boltzmann method,” *EPL (Europhysics Letters)* **47**, 182 (1999).
- ³³P. Lallemand and L.-S. Luo, “Theory of the lattice Boltzmann method: Dispersion, dissipation, isotropy, Galilean invariance, and stability,” *Physical review E* **61**, 6546 (2000).
- ³⁴S. Succi, *The Lattice Boltzmann Equation for Fluid Dynamics and Beyond* (Oxford University Press, 2001).
- ³⁵T. Krüger, H. Kusumaatmaja, A. Kuzmin, O. Shardt, G. Silva, and E. M. Viggien, “The lattice Boltzmann method,” *Springer International Publishing* **10**, 978–3 (2017).
- ³⁶P. Lallemand, L.-s. Luo, M. Krafczyk, and W.-A. Yong, “The lattice Boltzmann method for nearly incompressible flows,” *Journal of Computational Physics* **431**, 109713 (2021).
- ³⁷O. Malaspinas and P. Sagaut, “Wall model for large-eddy simulation based on the lattice Boltzmann method,” *Journal of Computational Physics* **275**, 25–40 (2014).
- ³⁸J. Latt, B. Chopard, O. Malaspinas, M. Deville, and A. Michler, “Straight velocity boundaries in the lattice Boltzmann method,” *Physical Review E* **77**, 056703 (2008).
- ³⁹A. Musker, “Explicit expression for the smooth wall velocity distribution in a turbulent boundary layer,” *AIAA Journal* **17**, 655–657 (1979).
- ⁴⁰M. Haussmann, A. C. Barreto, G. L. Kouyi, N. Rivière, H. Nirschl, and M. J. Krause, “Large-eddy simulation coupled with wall models for turbulent channel flows at high Reynolds numbers with a lattice Boltzmann method: Application to Coriolis mass flowmeter,” *Computers & Mathematics with Applications* **78**, 3285–3302 (2019).
- ⁴¹H. Maeyama, T. Imamura, J. Osaka, and N. Kurimoto, “Unsteady turbulent flow simulation using lattice Boltzmann method with near-wall modeling,” in *AIAA Aviation 2020 Forum* (2020) p. 2565.
- ⁴²S. Wilhelm, J. Jacob, and P. Sagaut, “A new explicit algebraic wall model for LES of turbulent flows under adverse pressure gradient,” *Flow, Turbulence and Combustion* **106**, 1–35 (2021).
- ⁴³Y. Kuwata and K. Suga, “Wall-modeled large eddy simulation of turbulent heat transfer

- by the lattice Boltzmann method,” *Journal of Computational Physics* **433**, 110186 (2021).
- ⁴⁴X. Xue, H.-D. Yao, and L. Davidson, “Wall-modeled large-eddy simulation integrated with synthetic turbulence generator for multiple-relaxation-time lattice Boltzmann method,” *Physics of Fluids* **35** (2023).
- ⁴⁵M. L. Shur, P. R. Spalart, M. K. Strelets, and A. K. Travin, “A hybrid RANS-LES approach with delayed-DES and wall-modelled LES capabilities,” *International Journal of Heat and Fluid Flow* **29**, 1638–1649 (2008).
- ⁴⁶X. Xue, H.-D. Yao, and L. Davidson, “Synthetic turbulence generator for lattice Boltzmann method at the interface between rans and LES,” *Physics of Fluids* **34**, 055118 (2022).
- ⁴⁷S. Hoyas and J. Jiménez, “Scaling of the velocity fluctuations in turbulent channels up to $Re \tau = 2003$,” *Physics of Fluids* **18**, 011702 (2006).
- ⁴⁸M. Lee and R. D. Moser, “Direct numerical simulation of turbulent channel flow up to $Re \tau \approx 5200$,” *Journal of Fluid Mechanics* **774**, 395–415 (2015).
- ⁴⁹A. Pasquali, M. Geier, and M. Krafczyk, “Near-wall treatment for the simulation of turbulent flow by the cumulant lattice Boltzmann method,” *Computers & Mathematics with Applications* **79**, 195–212 (2020).
- ⁵⁰D. d’Humières, “Multiple-relaxation-time lattice Boltzmann models in three dimensions,” *Philosophical Transactions of the Royal Society of London. Series A: Mathematical, Physical and Engineering Sciences* **360**, 437–451 (2002).
- ⁵¹Z. Guo, C. Zheng, and B. Shi, “Discrete lattice effects on the forcing term in the lattice Boltzmann method,” *Physical review E* **65**, 046308 (2002).
- ⁵²J. Smagorinsky, “General circulation experiments with the primitive equations: I. the basic experiment,” *Monthly Weather Review* **91**, 99–164 (1963).
- ⁵³Y. Koda and F.-S. Lien, “The lattice Boltzmann method implemented on the gpu to simulate the turbulent flow over a square cylinder confined in a channel,” *Flow, Turbulence and Combustion* **94**, 495–512 (2015).
- ⁵⁴K. Abe, T. Kondoh, and Y. Nagano, “A new turbulence model for predicting fluid flow and heat transfer in separating and reattaching flows—I. Flow field calculations,” *International journal of heat and mass transfer* **37**, 139–151 (1994).
- ⁵⁵L. Davidson, “pyCALC-LES: A python code for DNS, LES and hybrid LES-RANS,” Chalmers University of Technology, Gothenburg (2021).
- ⁵⁶L. Olson and J. Schroder, “PyAMG: Algebraic multigrid solvers in Python v4. 0,” URL

<https://github.com/pyamg/pyamg>. Release 4 (2018).

V. ACKNOWLEDGEMENTS

We acknowledge funding support from European Commission CompBioMed Centre of Excellence (Grant No. 675451 and 823712). Support from the UK Engineering and Physical Sciences Research Council under the projects “UK Consortium on Mesoscale Engineering Sciences (UKCOMES)” (Grant No. EP/R029598/1) and “Software Environment for Actionable and VVUQ-evaluated Exascale Applications (SEAVEA)” (Grant No. EP/W007711/1) is gratefully acknowledged. We kindly acknowledge the funding from Chalmers Transport Area of Advance.

VI. DECLARATION OF INTERESTS

The authors declare that they have no known competing financial interests or personal relationships that could have appeared to influence the work reported in this paper.

VII. MATERIAL AVAILABILITY

The training code and data set for sparse data and dense data can be found on University College London Centre for Computational Science GitHub page: <https://github.com/UCL-CCS/PINN-WM-LBM>.